Smart Structures and Systems, *Vol. 15, No. 5 (2015) 1233-1252*
DOI: http://dx.doi.org/10.12989/sss.2015.15.5.1233

Crack identification in post-buckled beam-type structures

Shapour Moradi*[1] and Peyman Jamshidi Moghadam[2]

[1]*Department of Mechanical Engineering, Shahid Chamran University, Ahvaz, 61357, Iran*
[2]*M.Sc. in Mechanical Engineering, Department of Mechanical Engineering, No. 3384, Sharifi St., Mahshahr, 63518, Iran*

(Received November 4, 2013, Revised April 20, 2014, Accepted April 27, 2014)

Abstract. This study investigates the problem of crack detection in post-buckled beam-type structures. The beam under the axial compressive force has a crack, assumed to be open and through the width. The crack, which is modeled by a massless rotational spring, divides the beam into two segments. The crack detection is considered as an optimization problem, and the weighted sum of the squared errors between the measured and computed natural frequencies is minimized by the bees algorithm. To find the natural frequencies, the governing nonlinear equations of motion for the post-buckled state are first derived. The solution of the nonlinear differential equations of the two segments consists of static and dynamic parts. The differential quadrature method along with an arc length strategy is used to solve the static part, while the same method is utilized for the solution of the linearized dynamic part and the extraction of the natural frequencies of the cracked beam. The investigation includes several numerical as well as experimental case studies on the post-buckled simply supported and clamped-clamped beams having open cracks. The results show that several parameters such as the amount of applied compressive force and boundary conditions influences the outcome of the crack detection scheme. The identification results also show that the crack position and depth can be predicted well by the presented method.

Keywords: crack detection; beam vibration; postbuckling; differential quadrature method; bees algorithm

1. Introduction

Cracks in a structure reduce its dynamic stiffness, and consequently affects other behaviors such as vibrations, buckling and postbuckling. On the other hand, the same conclusion can be drawn when the structure undergoes compressive loads. Therefore, when it experiences both, the consequences are much more complicated. In fact, when a vibrating structure undergoes a state if postbuckling, due to the high bending load condition, it becomes more susceptible to crack initiation. Such events may happen in engineering structures such as columns, drill strings or railway tracks due to working and environmental factors.

The problem of vibrations of post-bucked beams has been studied by many researchers using a variety of analytical and numerical methods. Nayfeh *et al.* (1995) analyzed the vibrational mode shape of buckled beams using analytical and experimental methods. They used the static buckling mode shape and found an exact solution for natural frequency as well as vibrational mode shape of

*Corresponding author, Associate Professor, E-mail: moradis@scu.ac.ir

http://www.techno-press.org/?journal=sss&subpage=8 ISSN: 1738-1584 (Print), 1738-1991 (Online)

the beam. Addessi *et al.* (2005a) investigated the vibration of a beam, having a concentrated mass at its mid span, around its post-buckled state. Postbuckling analysis carried out using extensible model, while the free vibration analysis was performed with inextensible model. They solved the problem using Galerkin discretization and finite element methods. Emam (2009) studied the static and dynamic response of post-buckled geometrically imperfect composite beams analytically. Santillan *et al.* (2006) solved the problem of small amplitude free vibration of heavy clamped-clamped beams around their post-buckled state using the shooting method, and verified their approach with experimental data. Neukirch *et al.* (2012) studied analytically and numerically the small amplitude in-plane vibrations of an elastic clamped-clamped rod around its post-buckled state using extensible and inextensible models. In addition, several authors have reported the static analysis of cracked beams under the compressive axial loads. Yazdchi and GowhariAnaraki (2008) used the massless rotational spring model to analyze the load carrying capacity of cracked columns for different boundary conditions. Ke *et al.* (2009) studied the postbuckling behavior of edge cracked Timoshenko beams made of FGM.

On the other hand, the crack detection in beam-type structures has been widely addressed in the literature. Sinha *et al.* (2002) used the finite element method and penalty function minimization to find the crack in beam structures. Razi *et al.* (2011) introduced several fatigue cracks in a free-free aluminum beam by cyclic load under a three-point bending configuration and used the empirical mode decomposition method to identify the crack position. Evaluating the first instantaneous frequency using Hilbert-Huang transform, Roveri and Carcaterra (2012) detected the damage in a bridge structure under a traveling load. Using the vibratory power estimated from the measured accelerations on a damaged beam, Huh *et al.*(2012) proposed a damage index to identify the crack. Zhong and Oyadiji (2007), Wu and Wang (2011) and Umesha *et al.* (2009) applied the wavelet transform to detect the crack in beams. Khorram *et al.* (2012) compared the performance of two wavelet based damage techniques to find the location and size of the crack in a beam subjected to moving loads. Moradi *et al.* (2011) used bees algorithm to detect the crack location and depth in a cantilever beam. They verified their approach numerically and experimentally. Buezas *et al.* (2011) applied the genetic algorithm to identify a transverse breathing crack in a beam-like structure. Taking into account the contact between the interfaces of the crack, Rosales *et al.* (2009) combined a power series technique and artificial neural networks to find the crack parameters in beam-like structures. VakilBaghmisheh *et al.* (2012) applied a hybrid particle swarm-Nelder-Mead optimization technique for crack identification in cantilever beams.

To the best of authors' knowledge, the problem of crack detection in beams under the state of postbuckling has not been addressed in the literature. Therefore, this paper aims to identify the crack parameters in such cases. The approach followed in this paper is to consider the crack detection practice as an optimization problem, and identify the crack parameters using an evolutionary algorithm. The cracked beam is modeled as two segments connected by a massless rotational spring, whose stiffness could be determined by the size of the crack. The crack is assumed to be open to avoid the nonlinear effects associated with the breathing crack model. The solution of the governing nonlinear equations of motion for the post-buckled state of segments consists of static and dynamic parts, both of which result in nonlinear differential equations. The differential quadrature (DQ) method has been used to solve the equilibrium and dynamic parts. Application of DQ to the static differential equations and their corresponding boundary and continuity conditions results in a nonlinear algebraic system of equations, which will be solved utilizing an arc length strategy. The method is then applied to the linearized dynamic differential equations of motion to obtain an eigenvalue problem whose solution gives the natural frequencies

and mode shapes of the beam. For the inverse problem of crack detection an objective function is defined and minimized by an evolutionary algorithm. The weighted sum of the squared errors between the measured and computed natural frequencies is used as the objective function. The optimization problem is then solved by a swarm-based evolutionary optimization technique, namely the bees algorithm. To ensure the integrity of the presented method, some numerical as well as experimental case studies are carried out on the simply supported and clamped-clamped cracked beams made of polyvinylchloride (PVC).

2. Modeling

2.1 Governing equations

Fig. 1 shows an elastic beam of length l, height h and width b, having an open-edge full-width crack, perpendicular to the beam's longitudinal axis. The crack with the depth of a is located at l_c from one end. The beam is subjected to an axial compressive force p at $x=l$.

With the assumption that the effect of the crack is only apparent in the immediate neighborhood, the cracked beam can be modeled as two separate uniform segments connected with a massless rotational spring at the crack location. Fig. 2(a) shows an element of the beam in its initial and deformed configuration. In the figure, s is the arc length of the deflection curve, u and w are the displacements of the beam element along the x and y axes, respectively. In addition, θ is the rotation with respect to the x axis, and u_0, w_0 and θ_0 are the initial displacements and rotation, respectively.

The free body diagram of a differential beam element under end loads is depicted in Fig. 2(b), where n, q and m are the axial and shear forces, and bending moment, respectively. Neglecting the damping effects, shear deformation and rotary inertia, the differential equations of motion for the beams' post-buckled state can be described by the following relations (Riessner 1972, Hua *et al.* 2008)

$$\begin{aligned}
&\frac{\partial w^j}{\partial s}=\left(1+\frac{n^j}{EA}\right)\sin\theta^j-\sin\theta_0^j, \qquad \frac{\partial u^j}{\partial s}=\left(1+\frac{n^j}{EA}\right)\cos\theta^j-\cos\theta_0^j,\\
&EI\left[\frac{\partial\theta^j}{\partial s}-\frac{\partial\theta_0{}^j}{\partial s}\right]-m^j=0, \qquad \frac{\partial m^j}{\partial s}+q^j=0, \qquad j=1,2\\
&\frac{\partial}{\partial s}\left(n^j\sin\theta^j\right)+\frac{\partial}{\partial s}\left(q^j\cos\theta^j\right)=\rho\,\ddot{w}^j, \quad \frac{\partial}{\partial s}\left(n^j\cos\theta^j\right)-\frac{\partial}{\partial s}\left(q^j\sin\theta^j\right)=\rho\,\ddot{u}^j
\end{aligned} \tag{1}$$

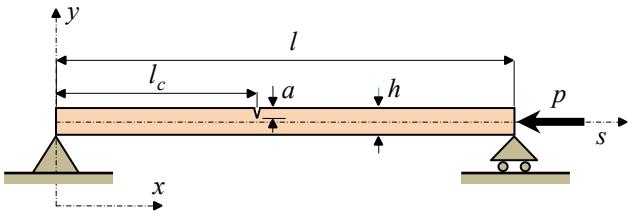

Fig. 1 Cracked beam under axial compressive load

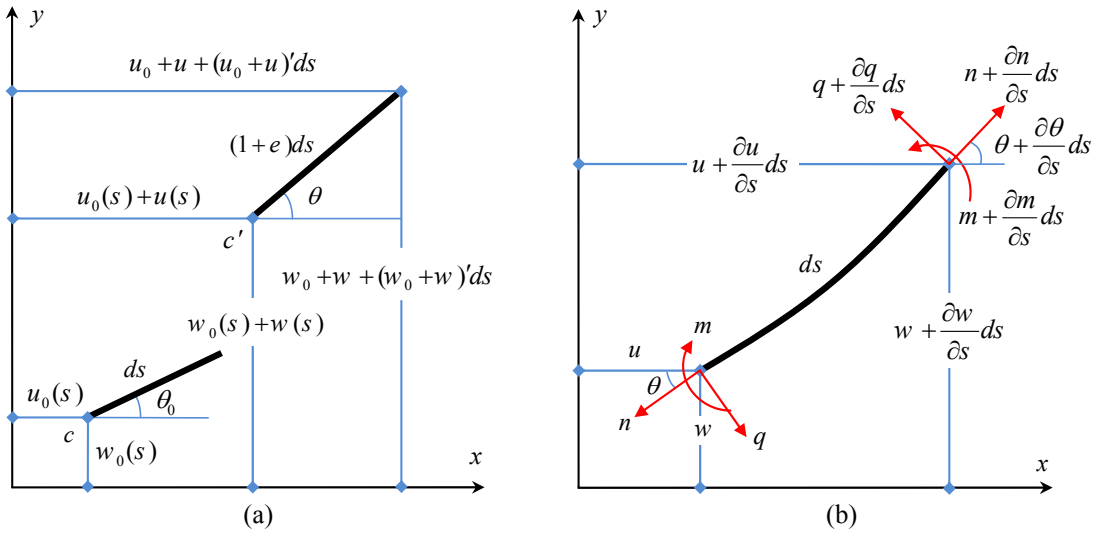

Fig. 2 (a) Deformation of an element and (b) Free body diagram of a differential beam element

where u^j and w^j are the displacements of jth beam along the x and y axes, respectively, θ^j is the rotation with respect to the x axis and dot means the derivative with respect to time. The first two equations represent the strain components of the element, the third equation corresponds to the constitutive equation, and the last three represent the governing differential equations of the motion. The cross section, A, and second moment of inertia, I, as well as Young's modulus, E, and Poisson's ratio, υ, are assumed to be similar for both sections. The analysis is carried out using the following dimensionless parameters

$$S=\frac{s}{l},\quad L=\frac{l}{l}=1,\quad L^j=\frac{l^j}{l},\quad K=\frac{Al^2}{I},$$
$$U^j=\frac{u^j}{l},\quad W^j=\frac{w^j}{l},\quad N^j=\frac{n^j l^2}{EI},\quad Q^j=\frac{q^j l^2}{EI},$$
$$M^j=\frac{m^j l}{EI},\quad P=\frac{pl^2}{EI},\quad T=\frac{t}{l^2}\sqrt{\frac{EI}{\rho}},\quad \Omega=\omega l^2\sqrt{\frac{\rho}{EI}}. \tag{2}$$

where ω, ρ and t are the vibration frequency, mass per unit length and time, respectively. Consequently, the governing equations can be written as

$$\frac{\partial W^j}{\partial S}=\left(1+\frac{N^j}{K}\right)\sin\theta^j-\sin\theta_0^j,\qquad \frac{\partial U^j}{\partial S}=\left(1+\frac{N^j}{K}\right)\cos\theta^j-\cos\theta_0^j,$$
$$\frac{\partial \theta^j}{\partial S}+\frac{\partial \theta_0^j}{\partial S}-M^j=0,\qquad \frac{\partial M^j}{\partial S}+Q^j=0,\qquad j=1,2$$
$$\frac{\partial}{\partial S}\left(N^j\sin\theta^j\right)+\frac{\partial}{\partial S}\left(Q^j\cos\theta^j\right)=\ddot{W}^j,\qquad \frac{\partial}{\partial S}\left(N^j\cos\theta^j\right)-\frac{\partial}{\partial S}\left(Q^j\sin\theta^j\right)=\ddot{U}^j \tag{3}$$

Considering the small amplitude vibrations around the post-buckled equilibrium configuration, the solution can be written as the sum of the equilibrium and harmonic parts in the following form

$$\begin{aligned}
U^j(S,T) &= U_e^j(S) + U_d^j(S)\sin\Omega T \\
W^j(S,T) &= W_e^j(S) + W_d^j(S)\sin\Omega T \\
\theta^j(S,T) &= \theta_e^j(S) + \theta_d^j(S)\sin\Omega T \\
N^j(S,T) &= N_e^j(S) + N_d^j(S)\sin\Omega T \\
Q^j(S,T) &= Q_e^j(S) + Q_d^j(S)\sin\Omega T \\
M^j(S,T) &= M_e^j(S) + M_d^j(S)\sin\Omega T
\end{aligned} \tag{4}$$

where indices *e* and *d* represent the equilibrium and dynamic states, respectively. In order to solve the vibration of the post-buckled beams, first the system of Eq. (3) is solved statically to determine the equilibrium shape. Eliminating the time related terms in Eq. (3), one can determine the following equilibrium equations

$$\begin{aligned}
&\frac{\partial W_e^j}{\partial S} = \left(1+\frac{N_e^j}{K}\right)\sin\theta_e^j - \sin\theta_0^j, && \frac{\partial U_e^j}{\partial S} = \left(1+\frac{N_e^j}{K}\right)\cos\theta_e^j - \cos\theta_0^j, \\
&\frac{\partial \theta_e^j}{\partial S} + \frac{\partial \theta_0^j}{\partial S} - M_e^j = 0, && \frac{\partial M_e^j}{\partial S} + Q_e^j = 0, \qquad j=1,2 \\
&\frac{\partial}{\partial S}\left(N_e^j \sin\theta_e^j\right) + \frac{\partial}{\partial S}\left(Q_e^j \cos\theta_e^j\right) = 0, && \frac{\partial}{\partial S}\left(N_e^j \cos\theta_e^j\right) - \frac{\partial}{\partial S}\left(Q_e^j \sin\theta_e^j\right) = 0
\end{aligned} \tag{5}$$

Next, the small vibrations around the post-buckled equilibrium are considered. Substituting Eqs. (4) into (3), and removing the nonlinear terms, the linear dynamic equations of motion can be obtained as

$$\begin{aligned}
&\frac{\partial W_d^j}{\partial S} = \left(1+\frac{N_e^j}{K}\right)\theta_d^j\cos\theta_e^j + \frac{N_d^j}{K}\sin\theta_e^j, && \frac{\partial U_d^j}{\partial S} = -\left(1+\frac{N_e^j}{K}\right)\theta_d^j\sin\theta_e^j + \frac{N_d^j}{K}\cos\theta_e^j, \\
&\frac{\partial \theta_d^j}{\partial S} - M_d^j = 0, && \frac{\partial M_d^j}{\partial S} + Q_d^j = 0, \qquad j=1,2 \\
&\frac{\partial}{\partial S}\left[N_d^j\sin\theta_e^j + N_e^j\theta_d^j\cos\theta_e^j\right] + \frac{\partial}{\partial S}\left[Q_d^j\cos\theta_e^j - Q_e^j\theta_d^j\sin\theta_e^j\right] = -\Omega^2 W_d^j \\
&\frac{\partial}{\partial S}\left[N_d^j\cos\theta_e^j - N_e^j\theta_d^j\sin\theta_e^j\right] - \frac{\partial}{\partial S}\left[Q_d^j\sin\theta_e^j + Q_e^j\theta_d^j\cos\theta_e^j\right] = -\Omega^2 U_d^j
\end{aligned} \tag{6}$$

2.2 Crack model

As mentioned in the preceding section, the cracked beam can be modeled as two separate segments connected with a rotational spring at the crack location (Fig. 3). In order to avoid the

nonlinear effects, the crack is also assumed to be open. This assumption is more acceptable when the beam is in post-buckled state. The bending moment has a direction so that its influence opens the crack. Therefore, the edges can be further separated for the cracks located on the outer surface of the beam.

The existence of the crack produces some local flexibility, which is a function of the dimensions and elastic properties of cracked region. Such flexibility results in geometric discontinuities around the crack sides. The flexibility coefficient, c, is calculated by making use of the relationship

$$c = \frac{\partial^2 W_b}{\partial m^2} \tag{7}$$

where W_b is energy of the elastic deformation caused by the crack and can be described by

$$W_b = \frac{b(1-\nu^2)}{E}\int_0^a K_I^2 d\alpha \tag{8}$$

K_I is the stress intensity factor under mode one bending load and is equal to

$$K_I = \left(\frac{6M_b}{bh^2}\right)\sqrt{\pi\alpha}F(\bar{\alpha}) \tag{9}$$

where M_b is the bending moment at the crack section, α varies through the depth of the crack and $\bar{\alpha} = \alpha / h$. The flexibility function $F(\bar{\alpha})$ is defined by the following relation (Saavedra and Cuitino 2001, Karaagac *et al.* 2009)

$$F(\bar{\alpha}) = \frac{\sqrt{\frac{2}{\pi\bar{\alpha}}\tan\frac{\pi\bar{\alpha}}{2}}\left[0.923 + 0.199\left(1-\sin\frac{\pi\bar{\alpha}}{2}\right)^4\right]}{\cos\left(\frac{\pi\bar{\alpha}}{2}\right)} \tag{10}$$

Combining Eqs. (7)-(10), the flexibility coefficient is obtained as

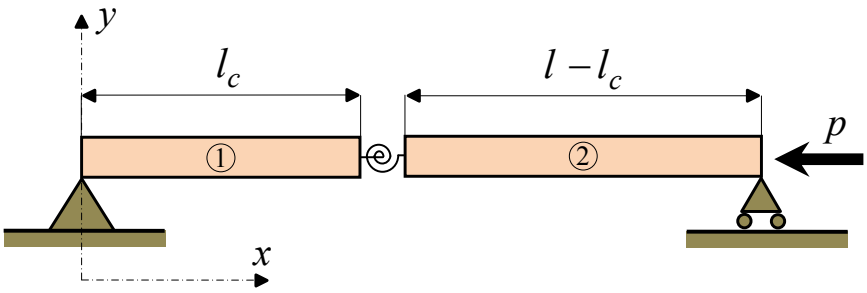

Fig. 3 Cracked beam modeled by a massless rotational spring

$$c=\frac{72\pi(1-\nu^2)}{E\,h^2\,b}\int_0^{\bar{a}}\bar{\alpha}F^2\left(\bar{\alpha}\right)d\bar{\alpha} \tag{11}$$

where $\bar{a}=a/h$.

2.3 Continuity and boundary conditions

The displacement, force and moment continuity conditions at the interface of the beam segments in equilibrium state are

$$\begin{aligned}&U_e^1\big|_{L_c}-U_e^2\big|_{L_c}=0,\quad W_e^1\big|_{L_c}-W_e^2\big|_{L_c}=0,\\&F_{ex}^1\big|_{L_c}-F_{ex}^2\big|_{L_c}=0,\quad F_{ey}^1\big|_{L_c}-F_{ey}^2\big|_{L_c}=0,\quad M_e^1\big|_{L_c}-M_e^2\big|_{L_c}=0,\end{aligned} \tag{12}$$

where $L_c=l_c/l$ and

$$F_{ex}^j=N_e^j\cos\theta_e^j-Q_e^j\sin\theta_e^j,\quad F_{ey}^j=N_e^j\sin\theta_e^j+Q_e^j\cos\theta_e^j \tag{13}$$

The same continuity conditions in the dynamic state are

$$\begin{aligned}&U_d^1\big|_{L_c}-U_d^2\big|_{L_c}=0,\quad W_d^1\big|_{L_c}-W_d^2\big|_{L_c}=0,\\&F_{dx}^1\big|_{L_c}-F_{dx}^2\big|_{L_c}=0,\quad F_{dy}^1\big|_{L_c}-F_{dy}^2\big|_{L_c}=0,\\&M_d^1\big|_{L_c}-M_d^2\big|_{L_c}=0,\end{aligned} \tag{14}$$

where

$$\begin{aligned}F_{dx}^j&=N_d^j\cos\theta_e^j-N_e^j\theta_d^j\sin\theta_e^j-Q_d^j\sin\theta_e^j-Q_e^j\theta_d^j\cos\theta_e^j,\\F_{dy}^j&=N_d^j\sin\theta_e^j+N_e^j\theta_d^j\cos\theta_e^j+Q_d^j\cos\theta_e^j-Q_e^j\theta_d^j\sin\theta_e^j.\end{aligned} \tag{15}$$

The change in the slope of the elastic curve at the crack position in equilibrium and dynamic states are given by

$$\theta_e^1\big|_{L_c}-\theta_e^2\big|_{L_c}=-\frac{EIc}{l}M_e^2\big|_{L_c} \tag{16}$$

$$\theta_d^1\big|_{L_c}-\theta_d^2\big|_{L_c}=-\frac{EIc}{l}M_d^2\big|_{L_c} \tag{17}$$

The displacement, slope and force boundary conditions at the simply supported ends in static and dynamic states are

$$\begin{aligned}&U_e^1\big|_{S=0}=0,\quad W_e^1\big|_{S=0}=0,\quad M_e^1\big|_{S=0}=0,\\&N_e^2\big|_{S=1}\cos(\theta_e^2\big|_{S=1})-Q_e^2\big|_{S=1}\sin(\theta_e^2\big|_{S=1})=P,\\&W_e^2\big|_{S=1}=0,\quad M_e^2\big|_{S=1}=0\end{aligned} \tag{18}$$

and

$$U_d^1\big|_{S=0}=0,\qquad W_d^1\big|_{S=0}=0,\qquad M_d^1\big|_{S=0}=0,$$
$$U_d^2\big|_{S=1}=0,\qquad W_d^2\big|_{S=1}=0,\qquad M_d^2\big|_{S=1}=0 \tag{19}$$

The same boundary conditions for a beam with clamped ends can be represented by

$$U_e^1\big|_{S=0}=0,\qquad W_e^1\big|_{S=0}=0,\qquad \theta_e^1\big|_{S=0}=0,$$
$$N_e^2\big|_{S=1}=P,\qquad W_e^2\big|_{S=1}=0,\qquad \theta_e^2\big|_{S=1}=0 \tag{20}$$

$$U_d^1\big|_{S=0}=0,\quad W_d^1\big|_{S=0}=0,\quad M_d^1\big|_{S=0}=0,$$
$$U_d^2\big|_{S=1}=0,\quad W_d^2\big|_{S=1}=0,\quad M_d^2\big|_{S=1}=0. \tag{21}$$

2.4 Differential quadrature implementation

The differential quadrature (DQ) method is utilized to solve both the nonlinear post-buckled equilibrium equations and linear dynamic equations of motion. The method states that the derivative of a function with respect to a space variable can be approximated by a weighted linear combination of function values at some intermediate points in the domain of that variable. Therefore, the first derivative of the function $f=f(x)$ at an intermediate point x_i can be represented as

$$\frac{\mathrm{d}f(x_i)}{\mathrm{d}\,x}=\sum_{j=1}^{n_p}C_{ij}f(x_j)\qquad i=1,\ldots,n_p \tag{22}$$

where n_p is the number of grid spacing and C_{ij} are the weighting coefficients for the first order derivatives given by (Shu and Richards 1992)

$$C_{ij}=\begin{cases}\dfrac{\prod(x_i)}{(x_i-x_j)\cdot\prod(x_j)} & (i\neq j)\\[2ex] -\displaystyle\sum_{\substack{j=1\\ j\neq i}}^{n_p}C_{ij} & (i=j)\end{cases} \tag{23}$$

where

$$\prod(x_i)=\prod_{\substack{j=1\\ j\neq i}}^{n_p}(x_i-x_j) \tag{24}$$

The following Gauss-Lobatto-Chebyshev grid points have been used to discretize each domain

$$x_i = X_0 + \frac{X_1}{2}\left(1-\cos\frac{(i-1)\pi}{n_p-1}\right) \qquad i=1,\ldots,n_p \tag{25}$$

where for the first segment X_0=0 and X_1=L_c, while for the second segment X_0=L_c and X_1=1-L_c. Application of the DQ method to the static post-buckled equations of (5) results in the following sets of nonlinear algebraic equations

$$\begin{aligned}
&\sum_{k=1}^{n_p} C_{ik}W_{ek}^j = \left(1+\frac{N_{ei}^j}{K}\right)\sin\theta_{ei}^j - \sin\theta_{0i}^j, \qquad \sum_{k=1}^{n_p} C_{ik}U_{ek}^j = \left(1+\frac{N_{ei}^j}{K}\right)\cos\theta_{ei}^j - \cos\theta_{0i}^j\\
&\sum_{k=1}^{n_p} C_{ik}\theta_{ek}^j + \left(\frac{\partial\theta_0^j}{\partial S}\right)_i - M_{ei}^j = 0, \qquad \sum_{k=1}^{n_p} C_{ik}M_{ek}^j - Q_{ei}^j = 0 \qquad i=1,2,\cdots,n_p-1;\quad j=1,2\\
&\sum_{k=1}^{n_p} C_{ik}N_{ek}^j\sin\theta_{ek}^j + \sum_{k=1}^{n_p} C_{ik}Q_{ek}^j\cos\theta_{ek}^j = 0, \qquad \sum_{k=1}^{n_p} C_{ik}N_{ek}^j\cos\theta_{ek}^j - \sum_{k=1}^{n_p} C_{ik}Q_{ek}^j\sin\theta_{ek}^j = 0
\end{aligned} \tag{26}$$

Discretizing the static post-buckled equations and their corresponding continuity and boundary conditions leads to a system of nonlinear algebraic equations. In this study, an arc-length algorithm, based on the work of Forde and Stiemer (1987), and Al-rasby (1991) is used to solve the nonlinear system of equations resulting from the application of DQ method.

Next, the small vibration of the cracked beam around the post-buckled equilibrium state is considered. Discretizing the system of Eq. (6) by the DQ method results in the following system of equations

$$\begin{aligned}
&\sum_{k=1}^{n_p} C_{ik}W_{dk}^j = \left(1+\frac{N_{ei}^j}{K}\right)\theta_{di}^j\cos\theta_{ei}^j + \frac{N_{di}^j}{K}\sin\theta_{ei}^j, \quad \sum_{k=1}^{n_p} C_{ik}U_{dk}^j = -\left(1+\frac{N_{ei}^j}{K}\right)\theta_{di}^j\sin\theta_{ei}^j + \frac{N_{di}^j}{K}\cos\theta_{ei}^j\\
&\sum_{k=1}^{n_p} C_{ik}\theta_{dk}^j - M_{di}^j = 0, \qquad \sum_{k=1}^{n_p} C_{ik}M_{dk}^j - Q_{di}^j = 0 \qquad j=1,2\\
&\sum_{k=1}^{n_p} C_{ik}\left(N_{dk}^j\sin\theta_{ek}^j + N_{ek}^j\theta_{dk}^j\cos\theta_{ek}^j\right) + \sum_{k=1}^{n_p} C_{ik}\left(Q_{dk}^j\cos\theta_{ek}^j - Q_{ek}^j\theta_{dk}^j\sin\theta_{ek}^j\right) = -\Omega^2 W_{di}^j\\
&\sum_{k=1}^{n_p} C_{ik}\left(N_{dk}^j\cos\theta_{ek}^j - N_{ek}^j\theta_{dk}^j\sin\theta_{ek}^j\right) - \sum_{k=1}^{n_p} C_{ik}\left(Q_{dk}^j\sin\theta_{ek}^j + Q_{ek}^j\theta_{dk}^j\cos\theta_{ek}^j\right) = -\Omega^2 U_{di}^j
\end{aligned} \tag{27}$$

The DQ method is also used to discretize the continuity and boundary conditions in the dynamic state, which, along with the above equations, results in a system of linear eigenvalue equations. The solution of this eigenvalue problem by a standard eigensolver provides the natural frequencies and corresponding modal shapes of the cracked post-buckled beam.

2.5 Crack detection

As described above, the natural frequencies of a cracked post-buckled beam are functions of the location and depth of the crack. Therefore, one could consider the crack detection procedure as an inverse problem and use experimental modal data to identify the cracks. An optimization algorithm can be applied to predict the crack parameters by searching for the optimum value of an

objective function. The location and depth of the crack can be regarded as the design variables, and the weighted sum of the squared errors between the measured and computed natural frequencies may be used as the objective or fitness function.

Optimization algorithms that are based on the random search are more effective in finding the global optimum than the classical gradient-based methods. There are some random search techniques such as evolutionary algorithms (EAs) (Ashlock 2006), which use global search methods inspired from natural evolution. Among these methods, biology inspired and swarm-based optimization algorithms are the most popular. These methods search from a population of solutions instead of relying on a single point. In this study, the bees algorithm (Moradi *et al.* 2011) has been used to minimize the fitness function. It is based on the food foraging behavior of swarms of honey bees. The method performs a neighborhood search combined with a random search and can be used for engineering optimization. It searches for the particular crack parameters (i.e., location and depth) which results in corresponding changes in natural frequencies amongst different possible solutions. The objective function, f, to be minimized is defined as

$$f\left(L_c, a_c\right) = \sum_{i=1}^{n} w_i \log\left(\frac{\Omega_i^m - \Omega_i}{\Omega_i^m}\right)^2 \tag{28}$$

where a_c is the crack depth to beam thickness ratio (i.e., a/h), Ω_i^m is the ith measured dimensionless natural frequency of the cracked beam, Ω_i refers to the ith numerical dimensionless natural frequency calculated by DQ, and $w_i$is the ith weighting factor. The first three natural frequencies of the beam (i.e., n=3) are used to construct the objective function. Additionally, in considering the random nature of the algorithm, the best results of 10 runs have been reported as the final result.

3. Results

To validate the algorithm presented in the last section, several numerical as well as experimental case studies were performed on simply supported and clamped-clamped cracked beams made of polyvinylchloride (PVC). Modulus of elasticity, Poisson's ratio, and density of the PVC beam are 3.7 Gpa, 0.4 and 1400 kg/m^3, respectively. Three kinds of beams with the dimensions specified in Table 1 are used throughout the study. The accuracy of the results is assessed by defining the following errors, which indicate the difference between the exact and the predicted crack parameters

$$\varepsilon_l = \left|L_{ce} - L_{cp}\right| \times 100, \qquad \varepsilon_h = \left|a_{ce} - a_{cp}\right| \times 100 \tag{29}$$

Table 1 Dimensions of the beams

No.	l (mm)	b (mm)	h (mm)
1	895	25	10
2	1000	25	10
3	775	20	10

where L_{ce} and L_{cp} are the exact and the predicted dimensionless crack positions, and a_{ce} and a_{cp} are the exact and the predicted crack depth ratios, respectively.

3.1 Numerically-simulated damage studies

In order to verify the robustness of the method, numerically-simulated cases with different damage parameters and end conditions were tested. First, a beam, whose material properties and dimensions are similar to beam No. 1 of Table 1, simply supported at both ends and undergoing 150 mm end shortening, was selected. The cracks were placed at different locations and depths, and the corresponding natural frequencies were calculated numerically. Fig. 4 shows the variation of the first eight natural frequencies of the beam having a crack with relative depth of 0.2 in terms of the compressive load. The figure shows that as the applied load increases from zero to the buckling load, all the frequencies are reduced smoothly. The same conclusion can be made after buckling, except for the first mode. The fundamental frequency changes rapidly with the increase in applied load; where for a compressive load of $1.1P_{cr}$, it exceeds the 8^{th} frequency. The first mode shape of the beam is the first symmetric stretching-bending mode, whereas the next seven modes are the bending mode shapes. Since the dynamic stretching-induced stiffness dominates the elastic bending stiffness, for the first mode the natural frequencies increase with the increase in applied load.

Therefore, at the state of postbuckling, the fundamental frequency has exceeded the amount of several higher frequencies. Since in this study the first three lowest frequencies have been measured and used in optimization algorithm, they are in fact corresponding to the second, third and fourth frequencies.

Then bees algorithm was employed to predict the crack parameters. Table 2 shows the outcome of the crack detection scheme.

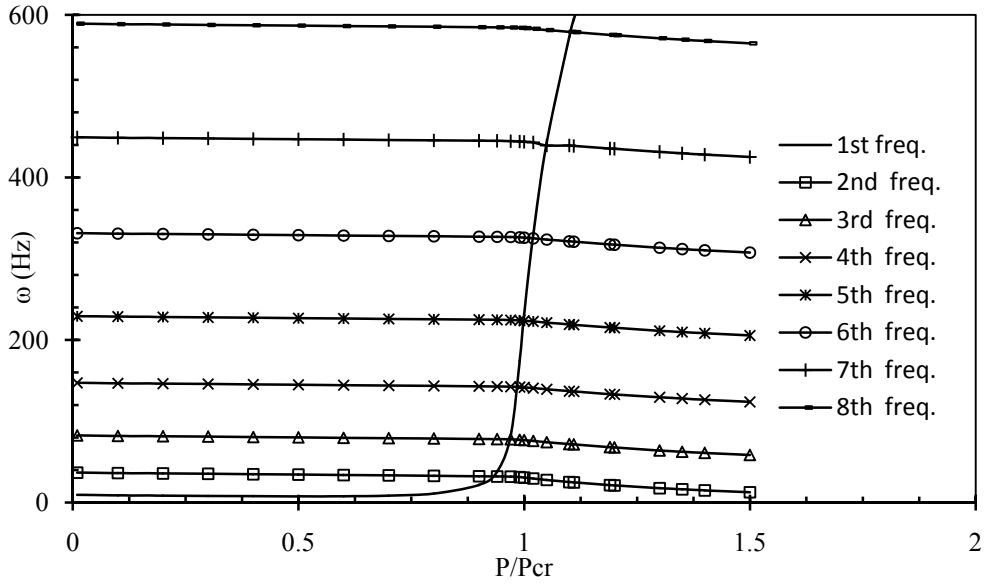

Fig. 4 The first 8 natural frequencies of simply supported cracked beam (a/h=0.2 and L_c=0.5)

Table 2 Prediction results of the numerical study for simply supported beam with 150 mm end shortening

P/P_{cr}	Exact crack		Predicted crack		Error %	
	L_c	a_c	L_c	a_c	ε_l	ε_a
1.087		0.1	0.29992	0.09997	0.008	0.003
1.083	0.3	0.2	0.29976	0.20025	0.024	0.025
1.076		0.3	0.30008	0.30002	0.008	0.002
1.086		0.1	0.39997	0.09996	0.003	0.004
1.081	0.4	0.2	0.40005	0.20002	0.005	0.002
1.071		0.3	0.40007	0.29999	0.007	0.001
1.086		0.1	0.50132	0.09998	0.132	0.002
1.078	0.5	0.2	0.49943	0.20002	0.057	0.002
1.069		0.3	0.50000	0.30001	0.000	0.001

It is observed from the table that the proposed method predicts the crack parameters very well. The maximum errors occur for the cases with small depth cracks. Moreover, it can be understood from the table that with fixed end shortening, the postbuckling load decreases conspicuously as the crack depth increases.

The effect of end shortening on crack identification is investigated in Table 3 for a simply supported beam made of beam No. 2, having a crack at its mid span and at different depths. The table shows that the postbuckling load is increased as the end shortening increases. The errors associated with crack identification are quite acceptable even for cracks with small depth ratios.

Table 3 Prediction results of the numerical study for simply supported beam with a crack at its mid span

End shortening	P/P_{cr}	Exact crack		Predicted crack		Error %	
		L_c	a_c	L_c	a_c	ε_l	ε_a
	1.107		0.1	0.49930	0.10004	0.070	0.004
200 mm	1.101		0.2	0.49728	0.19999	0.272	0.001
	1.091		0.3	0.50409	0.29894	0.409	0.106
	1.175		0.1	0.49996	0.10000	0.004	0.000
300 mm	1.169	0.5	0.2	0.50083	0.20002	0.083	0.002
	1.157		0.3	0.50315	0.30137	0.315	0.137
	1.253		0.1	0.49574	0.10009	0.426	0.009
400 mm	1.246		0.2	0.50354	0.19996	0.354	0.004
	1.234		0.3	0.49844	0.30002	0.156	0.002

Next, the effect of changing the end conditions is examined. The variation of the first four natural frequencies of a clamped-clamped beam, having a crack with the relative depth of 0.2, in terms of the applied load is computed numerically and demonstrated in Fig. 5.

For clamped-clamped beams, the odd frequencies increase rapidly just after the buckling while the even modes experience some decrement after the buckling (Neukirch *et al.* 2012). Moreover, when the beam undergoes large deflection after the buckling, the second, third and fourth natural frequencies decrease as the applied compressive load increases due to overall stiffness drop caused by the negative geometric stiffness. The fundamental frequency experiences a sharp growth immediately after the buckling load, and smoothly continues increasing with the increase in applied load. This is because the dynamic stretching-induced stiffness dominates the elastic bending stiffness, while for the other modes the bending stiffness is dominant (Addessi *et al.* 2005b). Therefore, the first natural frequency increases with the increase in applied load. The figure shows that at the state of postbuckling the amount of third frequency has been exceeded those of the first, second and forth frequencies. Again, as the first three lowest frequencies have been used in this study, they are in fact corresponding to the second, first and forth frequencies.

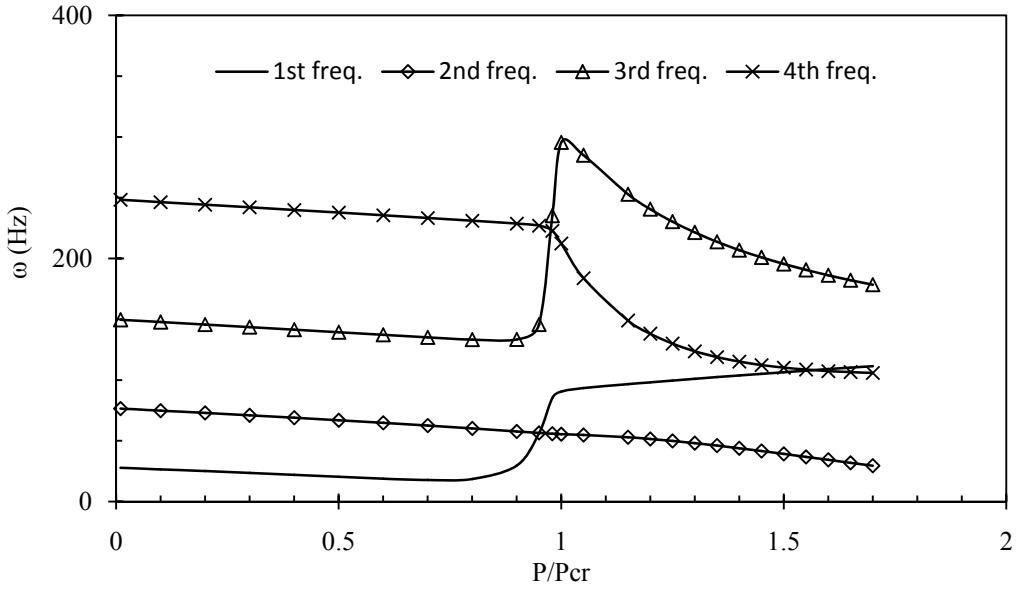

Fig. 5 The first four natural frequencies of clamped-clamped cracked beam

Table 4 Prediction results of the numerical study for clamped-clamped beam with 130 mm end shortening

P/P_{cr}	Exact crack		Predicted crack		Error %	
	L_c	a_c	L_c	a_c	ε_l	ε_a
1.0857		0.1	0.49794	0.10002	0.206	0.002
1.0783	0.5	0.2	0.50095	0.20000	0.095	0.000
1.0655		0.3	0.49866	0.30001	0.134	0.001

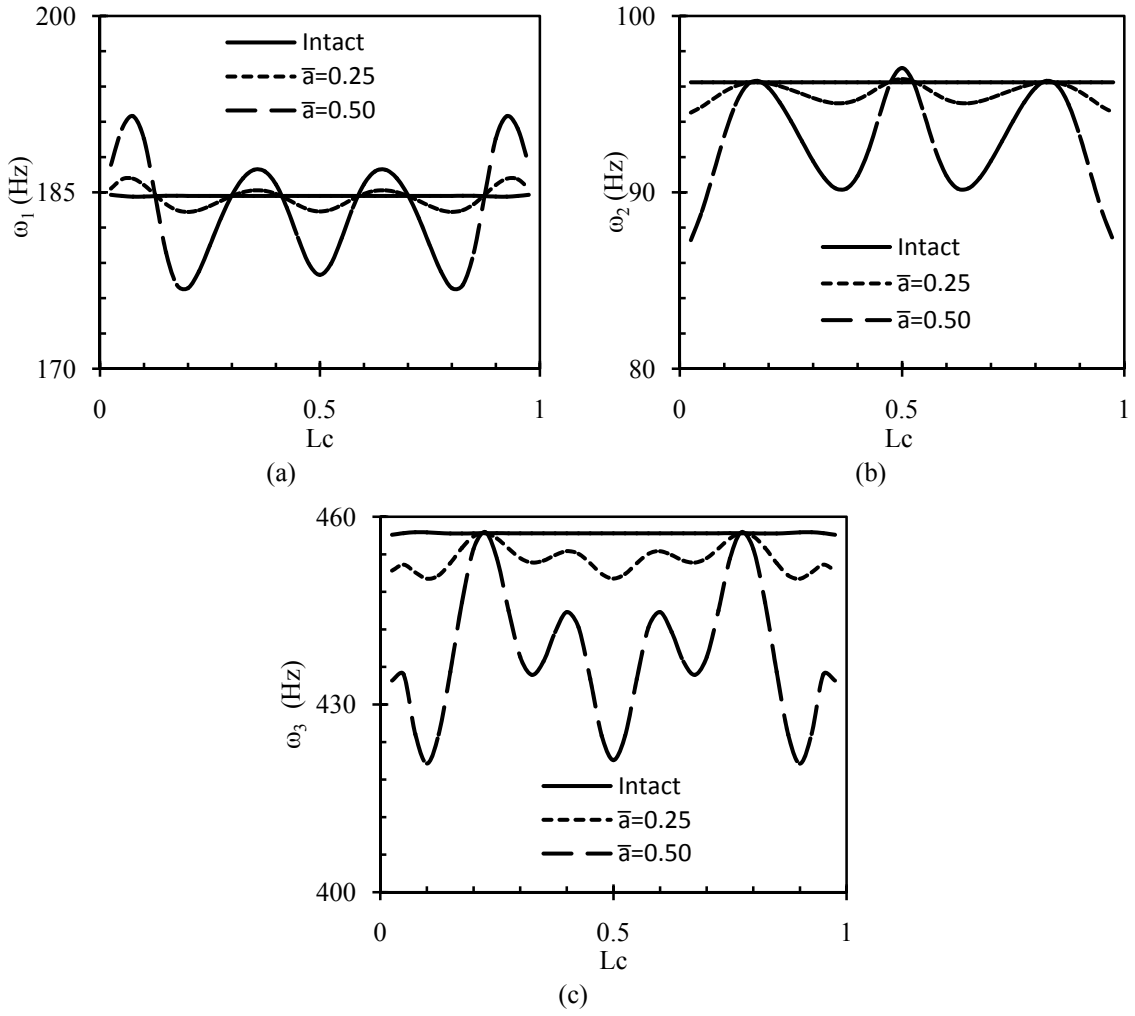

Fig. 6 Variation of the first three natural frequencies of the beam with the crack position for P/P_{cr}=1.2

The crack prediction study for beams with clamped ends is presented in Table 4. The end shortening is fixed at 130 mm for beam No. 3 of Table 1, having a crack at its mid span and at different depths. Again, the accuracy of the identification of crack parameters is excellent. The maximum error associated with the crack positions is less than 0.21%, while the maximum crack's depth prediction error is limited to 0.002%.

The effect of the crack location on the natural frequencies of the beam under the compressive load of $1.2P_{cr}$ is considered next. Fig. 6 shows the variation of the first three natural frequencies of a clamped-clamped beam, made of beam No. 3, as a function of the crack position for different crack depths. As illustrated in the figure, increasing the crack depth results in reduction in beam's stiffness and leads to the natural frequency decrement. Owing to the variation of bending moment throughout the beam, the change in frequency varies for different crack positions. Since the axial

compressive force exerted on the beam is fixed, any crack growth decreases the beam stiffness, increasing its end shortening and resulting in beam to be further bent. Therefore, it is expected that when the crack is positioned at certain points, the natural frequencies increase.

The variation of the first three natural frequencies of the beam under the compressive load of $1.2P_{cr}$ is plotted against the crack depth ratio for different crack positions in Fig. 7.

3.2 Experimental verification

To further verify the effectiveness of the presented approach, an experimental study was carried out on simply supported and clamped-clamped cracked beams. Mechanical properties and the dimensions of the test specimens were selected the same as those described in numerical simulation study. Different fixtures were used to represent the simply supported and clamped boundary conditions. Then, the load was applied to the beam to produce the state of postbuckling with certain amounts of end shortening. The data acquisition system consisted of a hammer (Global Test type AU02), a miniature accelerometer (B&K Type 4516), and a signal analyzer (B&K type 3032A) (see Fig. 8). These hardwares were utilized to measure the lowest three natural frequencies of the intact beams. Next, the open edge cracks were introduced by making fine saw cuts at different positions of the beam, perpendicular to the longitudinal axis and throughout the width.

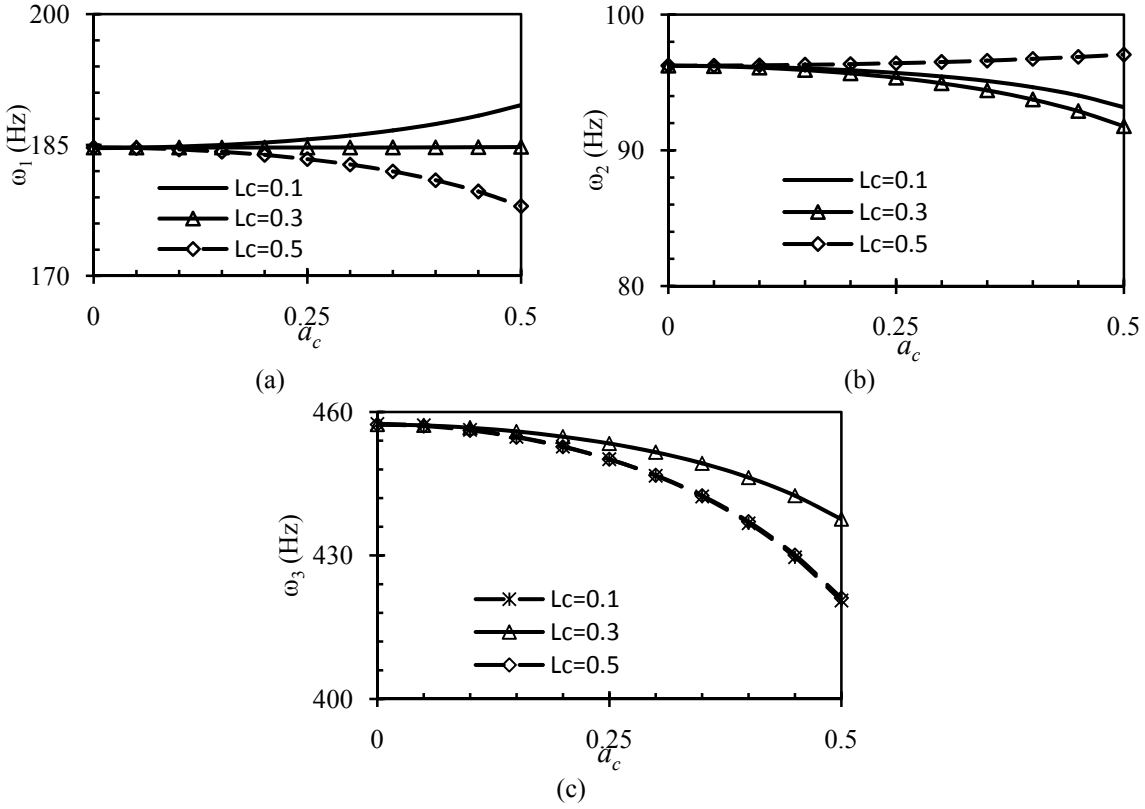

Fig. 7 Natural frequencies of the beam as a function of the crack depth for P/P_{cr}=1.2

As seen from the Fig. 8, the crack always remains open during the small amplitude vibration test. For simply supported ends, the generated cracks were in three relative locations (i.e., L_c=0.3, 0.4, 0.5) and three relative depths (i.e., a_c=0.1, 0.2, 0.3) of the beams. Fig. 9(a) shows a simply supported beam with a crack at its mid span in the postbuckling state.

At each step, the beam impacted with the hammer, and the three lowest natural frequencies of the cracked beams were measured. The corresponding natural frequencies of the cracked beams are presented in Table 5, referred as the cases 1-15, for different end shortenings.

Beam No. 1 has been used for the case numbers 1-6. For these cases, in which the cracks are not placed at the beam's mid span in the postbuckling state, the table shows that as the crack progresses through the depth of the beam, there is a reduction in beam's stiffness, leading to the natural frequency decrement. In addition, as the end shortening is fixed, stiffness reduction results in a decrease in applied compressive load and consequently a small increase in natural frequencies.

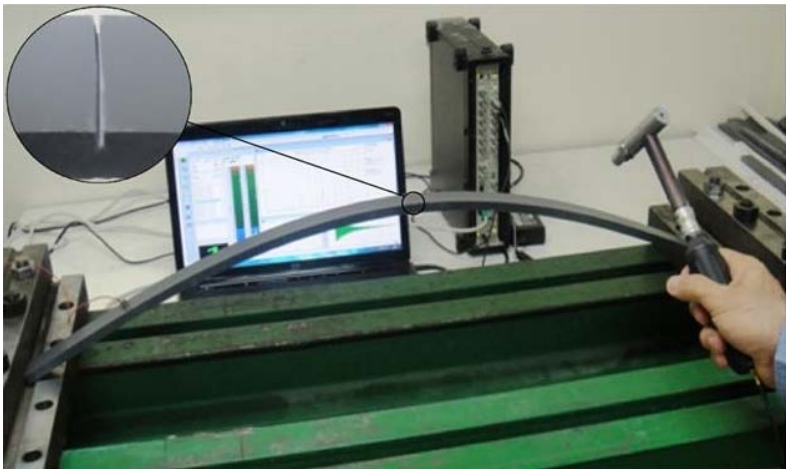

Fig. 8 Experimental setup

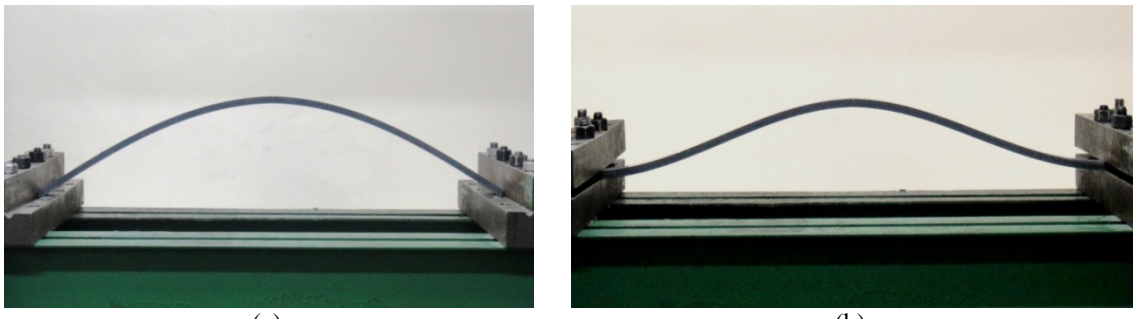

(a) (b)

Fig. 9 (a) Simply supported beam and (b) Clamped-clamped beam

Table 5 Experimental natural frequencies of cracked beams

Case no.	End shortening	Crack parameter		Frequency (Hz)		
		L_c	a_c	ω_1	ω_2	ω_3
1			0.1	26.470	73.250	136.450
2	150 mm	0.3	0.2	26.240	73.140	136.120
3			0.3	25.750	73.020	135.760
4			0.1	26.520	73.370	136.800
5	150 mm	0.4	0.2	26.330	73.190	136.200
6			0.3	25.890	72.660	134.000
7			0.1	20.120	56.860	108.730
8	200 mm	0.5	0.2	20.340	56.710	109.430
9			0.3	20.570	56.430	110.250
10			0.1	18.025	56.063	106.501
11	300 mm	0.5	0.2	18.203	55.874	106.672
12			0.3	18.457	55.560	107.012
13			0.1	15.790	52.875	104.672
14	400 mm	0.5	0.2	15.890	52.625	105.129
15			0.3	16.120	52.361	105.475
16			0.1	55.375	93.442	175.113
17	130 mm	0.5	0.2	55.752	92.985	174.651
18			0.3	56.428	92.677	174.752

Application of the proposed algorithm to the measured frequencies results in the prediction of the crack parameters, which are tabulated in the first six rows of Table 6. The table confirms the integrity of the proposed method. As shown in this table, the maximum crack position error is 5.1%. Also, the error associated with the prediction of the crack's depth is limited to 4.3%.

The next case study examines the effect of end shortening on the crack identification for beam No. 2, simply supported at both ends and having a crack at its mid span. The three lowest natural frequencies of the cracked beam are represented in Table 5, referred as the cases 7-15, for different end shortenings and crack depth ratios. It can be understood from the table that increasing the end shortening leads to a decrement in natural frequencies for a certain amount of crack depth ratio. However, for the first and third natural frequencies, which are correspond to the first and second

antisymmetric mode shapes, the crack coincides with a node at the mid spam of the beam, causing the beam to experience only the increase in natural frequencies due to the reduction of post-buckled axial load. Therefore, the crack propagation through the thickness results in increasing the first and third frequencies and decreasing the second frequencies.

The case number7 to15 of Table 6 summarize the crack prediction outcome. The maximum errors occurred in predicting the crack positions and depths are 3.9% and 3.7%, respectively. Again, the methodology used here successfully predicted the crack parameters even for high amounts of end shortening.

Table 6 Prediction results of the experimental study

Case no.	Exact crack		Predicted crack		Error %	
	L_c	a_c	L_c	a_c	ε_l	ε_a
1		0.1	0.257	0.136	4.3	3.6
2	0.3	0.2	0.336	0.229	3.6	2.9
3		0.3	0.265	0.330	3.5	3.0
4		0.1	0.358	0.134	4.2	3.4
5	0.4	0.2	0.429	0.177	2.9	2.3
6		0.3	0.451	0.343	5.1	4.3
7		0.1	0.461	0.132	3.9	3.2
8	0.5	0.2	0.527	0.186	2.7	1.4
9		0.3	0.535	0.329	3.5	2.9
10		0.1	0.531	0.129	3.1	2.9
11	0.5	0.2	0.473	0.218	2.7	1.8
12		0.3	0.468	0.333	3.2	3.3
13		0.1	0.536	0.136	3.6	3.6
14	0.5	0.2	0.477	0.223	2.3	2.3
15		0.3	0.539	0.337	3.9	3.7
16		0.1	0.458	0.129	4.2	2.9
17	0.5	0.2	0.537	0.230	3.7	3.0
18		0.3	0.443	0.342	5.7	4.2

The effect of changing the end conditions on crack prediction results is investigated next. For this test, a sample with the specification of beam No. 3 of Table 1 was considered; a beam with a crack at its mid span, clamped at both ends and compressed axially to produce a state of postbuckling with 130 mm end shortening (Fig. 9(b)). The corresponding natural frequencies of the cracked beam are presented in the last three rows of Table 5.

Also, the crack prediction results are given in the last three rows of Table 6. The highest errors occurred when detecting the crack with the relative depth of 0.3 (i.e., 5.7% and 4.2% for estimating the crack location and its depth, respectively). This means that the predicted crack location and its depth differ as much as 44.2 mm, and 0.42 mm from the exact ones, respectively.

4. Conclusions

In this study, the crack identification problem was investigated for beam-type structures under postbuckling state. The open crack, modeled by a rotational spring, divided the beam into two segments. For the forward problem, the solution consisted of the summation of the static and dynamic parts. The differential quadrature method along with an arc length strategy was used to solve the static part, while the same method and an eigensolver were utilized to solve the linearized dynamic part. For the inverse problem, a swarm-based evolutionary optimization technique, namely the bees algorithm, was used to minimize the weighted sum of the squared errors between the measured and computed natural frequencies, and to find the crack location and depth. Several numerical as well as experimental case studies on the post-buckled simply supported and clamped-clamped beams having an open crack were performed. The effect of several factors such as end shortening, boundary conditions, and position and depth of the cracks on the predicted crack parameters were investigated. The identification results show that the crack position and depth can be predicted well by the presented method. The investigation also showed that the boundary conditions as well as the amount of the applied compressive load highly affect the dynamic response of the structure and consequently the results of the crack detection scheme.

References

Addessi, D., Lacarbonara, W. and Paolone, A. (2005a), "Free in-plane vibrations of highly buckled beams carrying a lumped mass", *Acta Mech.*, **180**(1-4), 133-156.

Addessi, D., Lacarbonara, W. and Paolone, A. (2005b), "On the linear normal modes of planar pre-stressed curved beams", *J. Sound Vib*., **284**(3-5), 1075-1097.

Al-rasby, S.N. (1991), "Solution techniques in nonlinear structural analysis", *Comput. Struct.*, **40**(4), 985-993.

Ashlock, D. (2006), *Evolutionary computation for modeling and optimization*, Springer, NY, USA.

Buezas, F.S., Rosales, M.B. and Filipich, C.P. (2011), "Damage detection with genetic algorithms taking into account a crack contact model", *Eng. Fract. Mech.*, **78**(4), 695-712.

Emam, S.A. (2009), "A static and dynamic analysis of the postbuckling of geometrically imperfect composite beams", *Compos. Struct.*, **90**(2), 247-253.

Forde, B.W.R. and Stiemer, S.F. (1987), "Improved arc length orthogonality methods for nonlinear finite element analysis", *Comput. Struct.*, **27**(5), 625-630.

Hua, Y.J, Zhu, Y.Y. and Cheng, C.J. (2008), "DQEM for large deformation analysis of structures with discontinuity conditions and initial displacements", *Eng. Struct.*, **30**(5), 1473-1487.

Huh, Y.C, Chung, T.Y, Moon, S.J, Kil, H.G. and Kim, J.K. (2011), "Damage detection in beams using vibratory power estimated from the measured accelerations", *J. Sound Vib.*, **330**(15), 3645-3665.
Karaagac, C., Ozturk, H. and Sabuncu, M. (2009), "Free vibration and lateral buckling of a cantilever slender beam with an edge crack: Experimental and numerical studies", *J. Sound Vib.*, **326**(1-2), 235-250.
Ke, L.L, Yang, J. and Kitipornchai, K. (2009), "Postbuckling analysis of edge cracked functionally graded timoshenko beams under end shortening", *Compos. Struct.*, **90**(2), 152-160.
Khorram, A., Bakhtiari-Nejad, F. and Rezaeian, M. (2012), "Comparison studies between two wavelet based crack detection methods of a beam subjected to a moving load", *Int. J. Eng. Sci.*, **51**, 204-215.
Moradi, S., Razi, P. and Fatahi, L. (2011), "On the application of bees algorithm to the problem of crack detection of beam-type structures", *Comput. Struct.*, **89**(23-24), 2169-2175.
Nayfeh, A.H., Kreider, W. and Anderson, T.J. (1995), "Investigation of natural frequencies and mode shapes of buckled beams", *AIAA J.*, **33**(6), 1121-1126.
Neukirch, S, Frelat, J., Goriely, A. and Maurini, C. (2012), "Vibrations of post-buckled rods: the singular inextensible limit", *J. Sound Vib.*, **331**(3), 704-720.
Razi, P, Esmaeel, R.A. and Taheri, F. (2011), "Application of a robust vibration-based non-destructive method for detection of fatigue cracks in structures", *Smart Mater. Struct.*, **20**(11), 1-12.
Reissner, E. (1972), "On one-dimensional finite-strain beam theory: The plane problem", *J. Appl. Math. Phys.*, **23**(5), 795-804.
Rosales, M.B, Filipich, C.P. and Buezas, F.S. (2009), "Crack detection in beam-like structures", *Eng. Struct.*, **31**(10), 2257-2264.
Roveri, N. and Carcaterra, A. (2012), "Damage detection in structures under traveling loads by Hilbert-Huang transform", *Mech. Syst. Signal Pr.*, **28**, 128-144.
Saavedra, P.N. and Cuitino, L.A. (2001), "Crack detection and vibration behavior of cracked beams", *Comput. Struct.*, **79**(16), 1451-1459.
Santillan, S.T, Virgin, L.N. and Plaut, R.H. (2006), "Post-buckling and vibration of heavy beam on horizontal or inclined rigid foundation", *J. Appl. Mech.*, **73**(4), 664-671.
Shu, C. and Richards, B.E. (1992), "Application of generalized differential quadrature to solve two-dimensional incompressible navier-stokes equations", *Int. J. Numer. Meth. Fl.*, **15**(7), 791-798.
Sinha, J., Friswell, M. and Edwards, S. (2002) "Simplified models for the location of cracks in beam structures using measured vibration data", *J. Sound Vib.*, **251**(1), 13-38.
Umesha, P.K, Ravichandran, R. and Sivasubramanian, K. (2009), "Crack detection and quantification in beams using wavelets", *Comput. -Aided Civil Infrastruct. Eng.*, **24**(8), 593-607.
VakilBaghmisheh, M.T., Peimani, M., Sadeghi, M.H., Ettefagh, M.M. and FakheriTabrizi, A. (2012), "A hybrid particle swarm-nelder-mead optimization method for crack detection in cantilever beams", *Appl. Soft Comput.*, **12**(8), 2217-2226.
Wu, N. and Wang, Q. (2011), "Experimental studies on damage detection of beam structures with wavelet transform", *J. Eng. Sci.*, **49**(3), 253-261.
Yazdchi, K. and GowhariAnaraki, A.R. (2008), "Carrying capacity of edge-cracked columns under concentric vertical loads", *Acta Mech.*, **198**(1-2), 1-19.
Zhong, S. and Oyadiji, O. (2007), "Crack detection in simply supported beams without baseline modal parameters by stationary wavelet transform", *Mech. Syst. Signal Pr.*, **21**(4), 1853-1884.

CC